Takuma and Kase *Robomech J (2017) 4:9*
DOI 10.1186/s40648-017-0078-2

ROBOMECH Journal

RESEARCH ARTICLE Open Access

Influence of trunk structure on posture transition from quadrupedalism to bipedalism

Takashi Takuma* and Wataru Kase

Abstract

An effective strategy for walking over rough terrain, flat plane, and wreckage includes transitioning from quadrupedal to bipedal locomotion. In this study, we designed a trunk mechanism that provides successful posture transition from quadrupedalism to bipedalism. The proposed trunk mechanism imitates the human trunk with redundant joints and elastic muscles supporting the trunk. The simulation results show that the proposed mechanism provides a successful and more rapid transition compared to the conventional rigid body.

Keywords: Posture transition, Quadrupedalism, Bipedalism, Trunk mechanism

Background

Morphological transition, a posture transition between quadrupedalism and bipedalism is an important strategy for locomotion over rough terrain and rubble and working in such environments. In particular, quadrupedalism, which avoids tumble is suitable for walking over rough terrain [1, 2] and dynamic locomotion [3, 4]. In the contract, bipedalism is suitable for walking over flat or small convex and concave terrains [5, 6], obtaining a higher viewpoint, working in the standing position, or bridging a barrier. Therefore, it is important to achieve quick transition from quadrupedalism to bipedalism. There are some approaches toward achieving posture transition between quadrupedal and bipedal locomotion [7–11]. In [7, 8], authors proposed controllers for the transition utilizing Central Pattern Generator. In [9, 10], strategies were proposed for the transition. To our knowledge, few studies have discusses faster transition. Although a faster transition is proposed in [11], it required a complete motion including ankle and knee joints. By considering that a quicker transition requires the swinging up/down of the upper body while limbs are moving for locomotion, we discuss the quicker transition utilizing minimum set of joint actuation.

*Correspondence: takashi.takuma@oit.ac.jp
Osaka Institute of Technology, 5-16-1 Omiya, Asahi-ku, Osaka, Osaka, Japan

A dynamic trunk with a larger mass and inertia relative to the entire body is an important factor for the transition mechanism. During quadruped walking, the animal's or robot's trunk is located between its fore and hind legs. During bipedal walking, the trunk is located above the lower limbs. Therefore, the pathway of the trunk is longer than that of the other parts, and for a quicker transition, a higher acceleration or deceleration that significantly influences the transition stability is required. To achieve quicker transition, one strategy is to utilize a feedback controller that determines the location of the limbs and arms by using precise sensing and a robot model [11], and the other strategy is to design a suitable trunk mechanism that provides mechanical transition without the feedback controller. In this study, the second strategy is adopted and a suitable trunk mechanism, providing successful posture transition with minimum number of sensors and actuators, is designed.

Conventional bipedal and quadrupedal robots have a rigid body [1–8, 11]. However, their transition is significantly influenced by the trunk's large inertia, locus, center of mass, and large acceleration or deceleration during the quick transition. By adding joints on the trunk and bending and flexing the trunk at appropriate periods, the robot is expected to transition between bipedalism and quadrupedalism without falling down even during quick transition. For a simple posture transition from quadrupedalism to bipedalism, an animal-like trunk mechanism with viscoelastic joints is adopted. Although some studies

have examined the effect of a trunk mechanism with viscoelastic joints on quadrupedalism [12–14] and bipedalism [15], they do not discuss about the effect on the transition. Therefore, in this study, we designed a model that adopts the animal-like trunk mechanism in a simulation and observed the effect on the transition from posture of quadrupedalism to that of bipedalism. We focus on the influence of the elasticity of the trunk joints on the possibility of the transition and the allowable value of the transition velocity. By tuning the elasticity, the robot is expected to achieve successful and quick transformation without using sensors, actuators, and controllers.

Simulation model

Figure 1 shows the model of morphological transition from quadrupedalism to bipedalism. The model does not move on the frontal plane because we assume that the transition is operated symmetrically, and then the transition is operated on a sagittal plane. The robot has a foot, leg, trunk, and head. The mass of its fore leg (arm) is included in its upper body weight even though the inertia is ignored. This paper aims to obtain a quicker transition from quadrupedalism to bipedalism. We do not suppose that the locomotion halts for the transition but that the trunk is swung up while other limbs are moving for the locomotion. Therefore, we assumed that knee and ankle joints drive only for the locomotion, and a hip joint, as a minimum set of the active joint, is adopted to swing up the upper body.

Figure 2 shows schematic trajectories of the desired value or state of the hip, trunk, and foot. T_s indicates the transition period in which the hip joint rotates to swing up the upper body. The reminder of this section details each part.

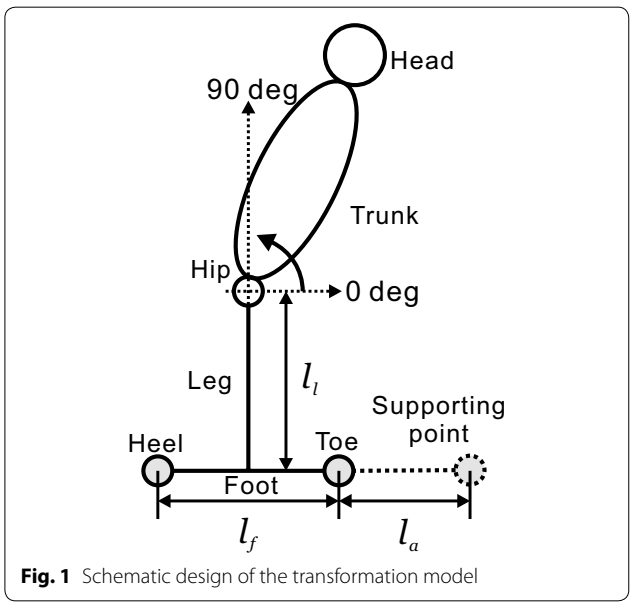

Fig. 1 Schematic design of the transformation model

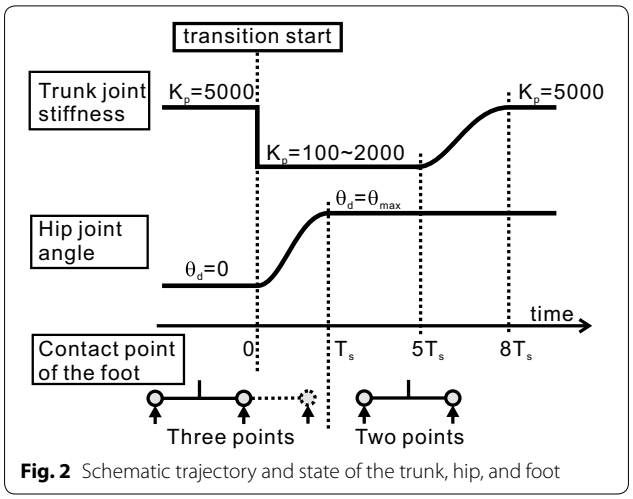

Fig. 2 Schematic trajectory and state of the trunk, hip, and foot

Trunk configuration

To observe the influence of the joint configuration on the performance of the transition, this study considers four trunk mechanisms including three passive joints, as shown in Fig. 3a (Model A), (b) (Model B), and (c) (Model C), and (d) (Rigid body). The joints in Fig. 3a–c follow spring-damper models. The ratios of the links of Models

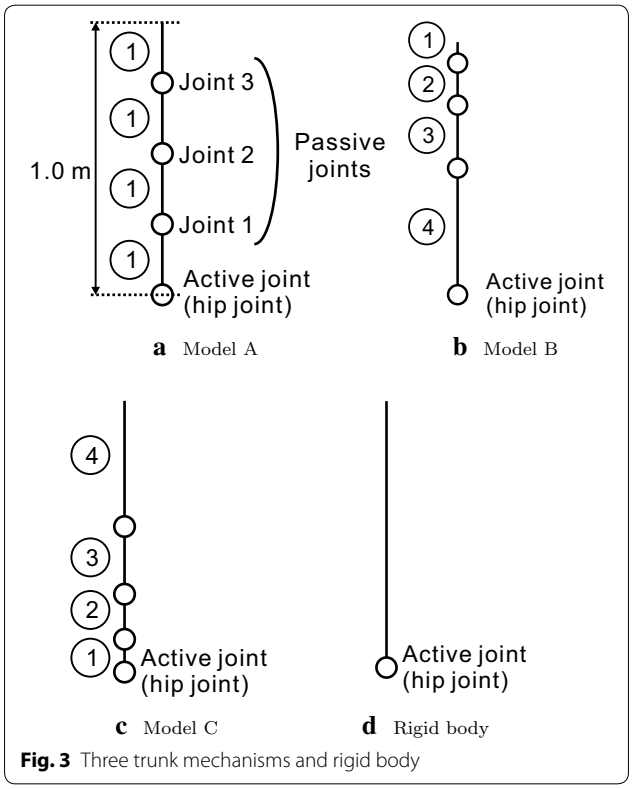

Fig. 3 Three trunk mechanisms and rigid body

A, B, and C are 1:1:1:1, 4:3:2:1, and 1:2:3:4 from bottom to top, respectively. The weight of each link is proportional to its length. For the development of the physical robot in future, the length and mass of the links should be practical to prepare, for example, for maintenance. The smallest link of the model is one of the trunk links of Models B and C: tips of the trunk in Model B and bottom of the trunk in Model C. We then set the length of the link as 0.1 m. Therefore, total length of trunk is 1.0 m. The weight of the smallest link of the trunk is set as 4 kg, which includes sensors and computer to measure the posture of the link and mechanism to switch viscoelasticity. Therefore, total weight of the trunk is 40 kg, and by including weight of a 5 kg head, referring human body weight ratio (head:trunk + arm = 8:60%) [16], the total weight of the upper limb is set as 45 kg.

The trunk joints have the following spring-damper characteristics:

$$\tau_i = -K_p\theta_i - K_d\dot{\theta}_i,$$

where θ_i and τ_i are the angle and torque applied to the i-th trunk joint, respectively. K_p is the elastic coefficient and K_d is the viscous coefficient. This allows the trunk to be flexible with viscoelasticity. In a test trial of the transition, we determined that the elastic coefficient should be switched according to the phase of the transition. Before the transition, a higher elastic coefficient is needed to keep the trunk horizontal. After the transition, when the center of the mass of the trunk moves to a higher position in case of successful transition, the higher spring coefficient is also needed to keep the trunk vertical. Therefore, as shown in Fig. 2, the coefficient K_p is set higher at 5000.0 Nm/rad just before the transition, and switched to be lower for $5T_s$ when the transition begins. It is then gradually changed higher as 5000.0 Nm/rad following sinusoidal function from $5T_s$ to $8T_s$ In the simulation, K_p is changed from 100 to 2000 Nm/rad by 100 Nm/rad. K_d is fixed at 10.0 Nm/(rad/s). We developed a physical trunk mechanism in which the joint viscoelasticity changes [17]. In [17], a trunk is constructed using rigid blocks made of chemical wood and viscoelastic discs made of rubber. A string is passed through the blocks and discs, and the viscoelasticity switches by the changing tensional force of the string. To change the tensional force, a feedback controller and an actuator are required. Except this feedback mechanism, the proposed mechanism does not require any feedback controller to stabilize the transition if we adopt our trunk mechanism.

Hip joint control

For the transition from quadrupedalism to bipedalism, the target angle θ_d of hip joint that swings up the trunk is set as follows (see Fig. 2):

$$\theta_d = \begin{cases} 0 & (t < 0) \\ \frac{\theta_{max}}{2} - \frac{\theta_{max}}{2}\cos\left(\pi\frac{t}{T_s}\right) & (0 \le t \le T_s) \\ \theta_{max} & (T_s < t) \end{cases},$$

where θ_{max} is the initial angle of the hip joint, and T_s indicates time period of the transition. Note that the hip joint follows the desired trajectory; however, the trunk oscillates even after the hip joint converges to the desired angle. The joint is controlled by a PD feedback controller as

$$\widehat{\tau} = -\widehat{K_p}(\theta_h - \theta_d) - \widehat{K_d}\dot{\theta_h},$$

where $\widehat{\tau}$ is the joint torque, θ_h is the joint angle, and $\widehat{K_p}$ and $\widehat{K_d}$ are positive constants. In this study, they are set at 1.0×10^3 N/rad and 5.0 N/(rad/s), respectively.

Leg and foot configuration

The length of lower leg l_l is set as 1.0 m. The weight of the bottom limb is set the same as the upper body weight, that is, 45 kg. The length of the foot l_f is 0.5 m. The root of the leg corresponding to the ankle, although it does not rotate, is attached at the middle of the foot. Therefore, the length between the ankle and toe is 0.25 m, and it is similar with that for the human foot. However, the length between the ankle and heel is considerable more than that for a human foot, that is, 0.25 m. In the test trial, we found that the center of mass of the trunk accelerated backward, and induces falling backward. Therefore, the final angle of the hip joint should be explored under the condition that the production of the position of the center of mass is set within the foot's region in static state. The complete study of the final angle lies outside the scope of this paper. We then set the final angle of the hip joint vertical to the ground ($\theta_{max} = 90°$), and the length between the ankle and heel is set longer at 0.25m to avoid falling backward. Figure 4 shows a general leg model that has an ankle and knee joints. When the ankle and knee joints are fixed, the lower leg is considered as a rigid body. If the positions of "Heel", "Toe" and "Hip" that interact with other link or ground are same with Fig. 1, the model dealt in this paper and the general model with the fixed knee and hip joints are almost equivalent although they are not completely equivalent because the positions of the center of mass and inertias are different. The masses of the leg and foot are 40 and 5 kg, respectively. In the test trial, we found that an additional point is needed to support the body while the spring coefficient is set lower, assuming that the body is supported by a hand. Therefore, the foot is supported by two points at the toe and heel, and another supporting point is set over the tips of the foot to support the trunk at the beginning of the transition.

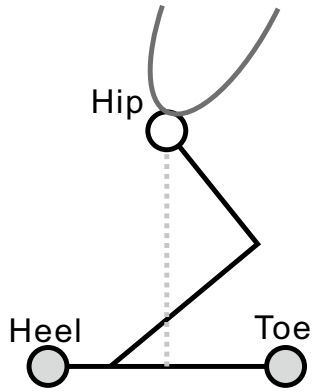

Fig. 4 Equilibrium posture with two models

The distance between the tips and the supporting point l_a is 0.5 m. The supporting point over the toe at the initial posture is disassembled after T_s (see Fig. 2). As explained earlier, the foot is supported by two points and an additional point for some time period. The contact model of point j is given by

$$F_{yj} = \begin{cases} -K_{tp}y_j - K_{td}\dot{y}_j & y_j < 0 \\ 0 & \text{else} \end{cases},$$

where F_{yj} is the vertical force, y_j is the height of the j-th contact point, and K_{tp} and K_{td} are the positive constants corresponding to spring and damping coefficients of the terrain. They are set as 1.0×10^4 N/m and 1.0×10^3 N/(m/s), respectively. The friction model of the contact point toward the horizontal direction is given by

$$F_xj = \begin{cases} -\mu F_{yj} - \widehat{K_{td}}\dot{x}_j & (\dot{x}_j \geq 0) \\ \mu F_{yj} - \widehat{K_{td}}\dot{x}_j & (\dot{x}_j < 0) \end{cases},$$

where F_xj is the horizontal force corresponding to coulomb and damping frictions on the j-th contact point. μ is a friction coefficient, and $\widehat{K_{td}}$ is damping coefficient. μ and $\widehat{K_{td}}$ are set as 0.4 and 1.0×10^3 N/(m/s), respectively.

Experiment

Demonstration of the transition

In this study, we used the simulation platform open dynamics engine (ODE) 0.13 running on Microsoft Visual Studio 2010. Figure 5 demonstrates successful transition when the joint elasticity of Model A is $K_p = 200$ Nm/rad and $T_s = 0.15$ s. When the time is T_s (between Fig. 5b, c), the desired hip joint is set to as $\theta_{max} = 90°$, and the supporting point over the toe is disassembled. When the time is $5T_s$ (between Fig. 5h, i), the elastic coefficient of the trunk joint begins to change from 200 to 5000 Nm/rad until time $8T_s$ (between Fig. 5m, n). As shown in the figures, the trunk passively oscillates and then becomes successfully upright. The point over the tip of the foot is not in contact after T_s, and the foot is supported by two points at the toe and heel. Figure 6 demonstrates a failed transition ($K_p = 200.0$ Nm/rad of Model C and $T_s = 0.15$ s) in which the hip joint does not swing up the trunk and the model falls ahead.

A simulation is conducted using various trunk joint elasticities K_p, from 100 to 2000 Nm/rad with 100 Nm/rad intervals from 0 s to $5T_s$ s, as explained in the previous section. For each joint elasticity, the transition time period providing successful transition is searched from 0.05 s to 5.0 s with intervals of 0.01 s. The viscous coefficient of the trunk joint K_d is fixed at 10.0 Nm/(rad/s).

Simulation results

Figure 7 shows the distribution of K_p and T_s providing successful transition of Model A. When the time period T_s is longer, the model achieves static transition in which the projection of a center of mass is always between a toe and heel. In contrast, when the period is appropriately shorter, as shown in the figure, the model achieves dynamic transition. Figure 8a shows magnified distribution at $0 \leq T_s \leq 0.75$ s, where the model with appropriate T_s achieves dynamic transition. It also indicates the range of time period providing transition of the rigid body. The rigid trunk achieves transition from 0.19 to 0.20 s. However, Model A with well-tuned elastic coefficient $K_p = 200$ Nm/rad achieves the quickest transition at $T_s = 0.11$ s: almost 42% shorter than that of the rigid body. Figure 8b, c show magnified distribution of Models B and C. As shown in the figures, Model B with an appropriate elastic coefficient also achieves quicker transition than the rigid body. However, Model C does not achieve a quicker transition even if the elastic coefficient is tuned. These results show that an appropriate design of the trunk whose joints are equally distributed or concentrated at the top achieves quicker transition than the rigid body without requiring an additional feedback controller to stabilize the faster transition but requiring one to change viscoelasticity of the trunk joints, in case of our physical trunk mechanism.

Figure 9a, b show trajectory of torque from 0.0 s to $2T_s$ when the trunk joint elasticity $K_p = 200$ Nm/rad and $T_s = 0.15$ s by which the model equipped with Model A obtains successful transition, while Model C fails. The statics show that a joint torque close to the root of the trunk is larger than that close to the tips of the trunk because the joint of trunk's root deforms by heavier mass and then it requires larger torque to swing up or support the heavier link chain. As shown in the figures, the peak of joint torque at the root of the joint (joint 1 in Fig. 1) is

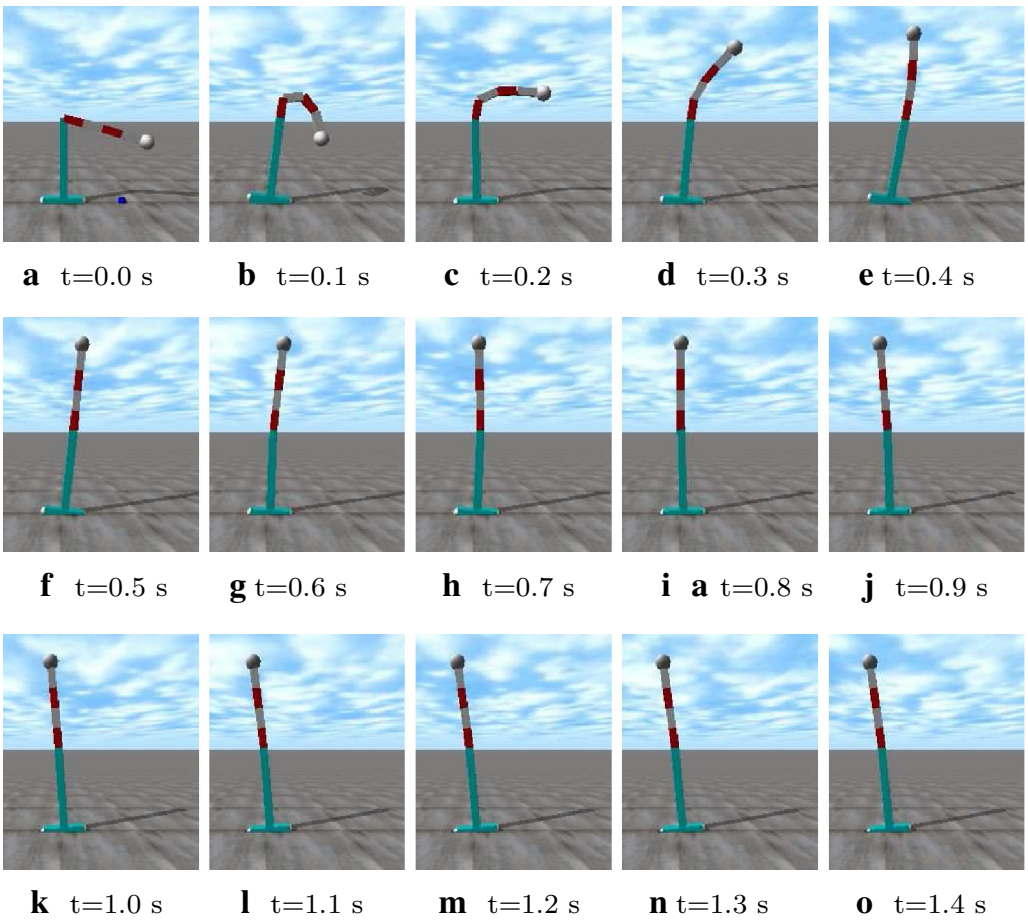

Fig. 5 Successful transition of Model A with $K_p = 200$ Nm/rad, $K_d = 10$ Nm/(rad/s), and $T_s = 0.1$ s

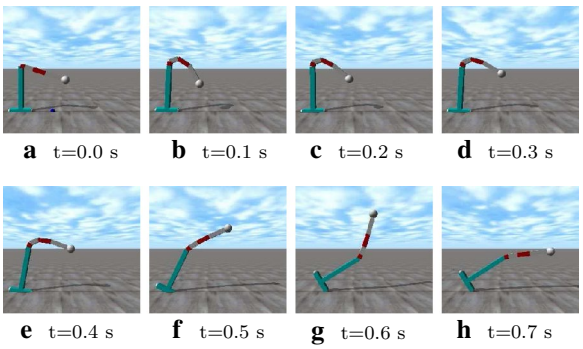

Fig. 6 Failed transition of Model C with $K_p = 200$ Nm/rad, $K_d = 10$ Nm/(rad/s), and 0.15 s

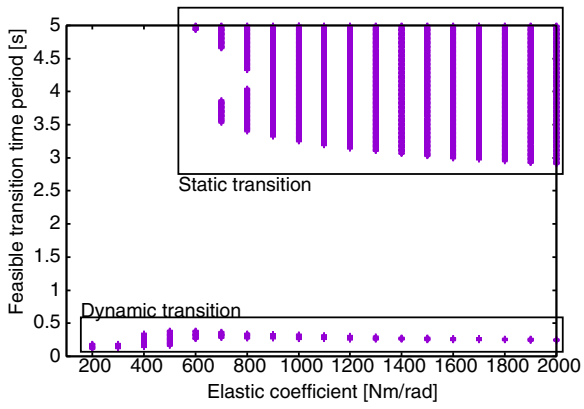

Fig. 7 Relationship between elastic coefficient and feasible time period of Model A transition

larger than that at the distal position of the trunk (joint 3). Therefore, in case of Model C, the joint at the distal position did not provide sufficient torque to lift up heavier link at the tips of the trunk: thus, the robot falls ahead. In Fig. 9a, the hip joint requires as large as 600 Nm, which an ordinal electric servo motor cannot generate. For the physical experiment, we expect a hydraulic actuator to provide such a considerable torque. Otherwise, the

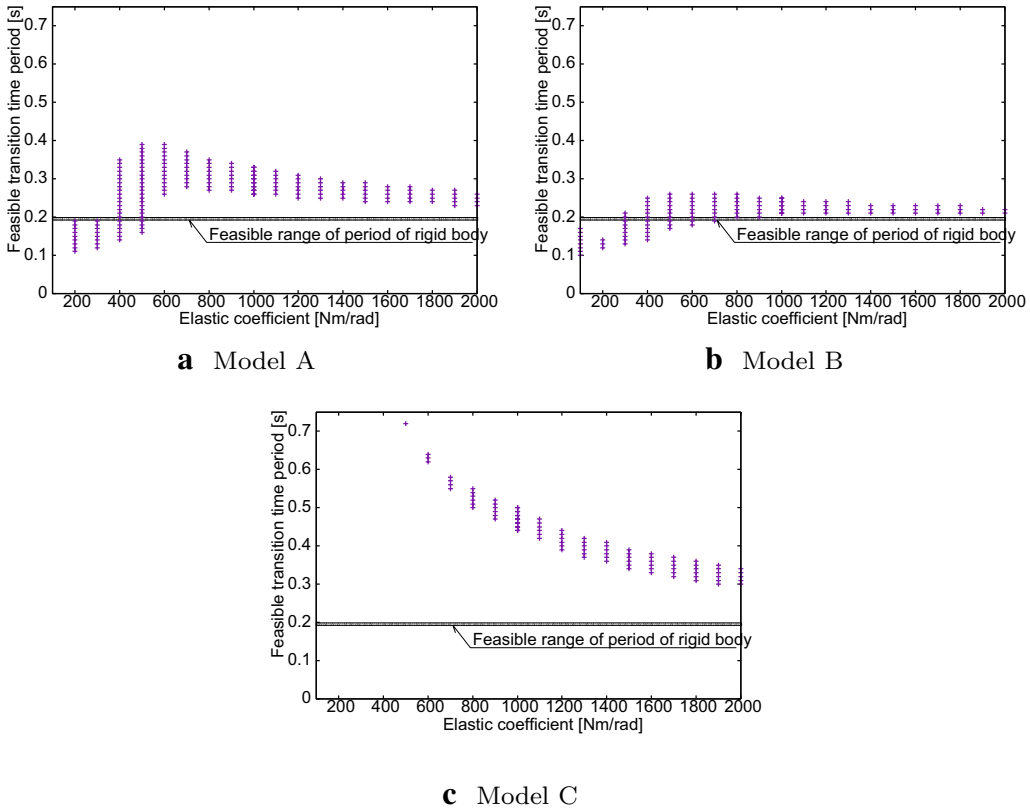

Fig. 8 Relationship between elastic coefficient and feasible time period of the transition by Model A, B, and C

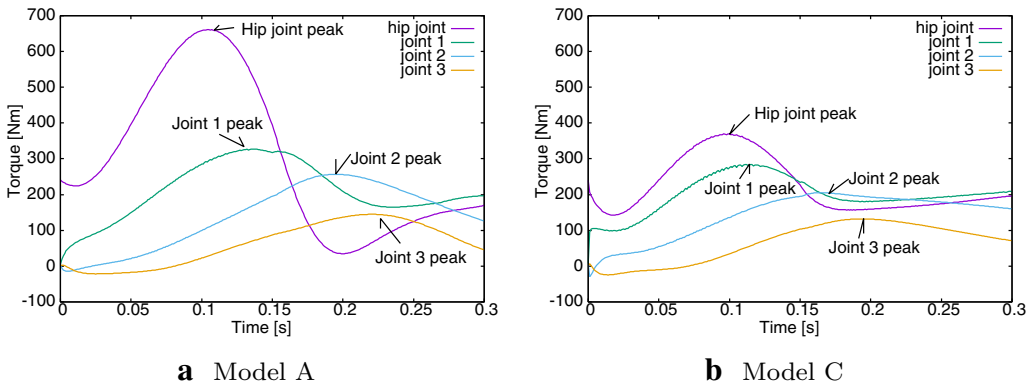

Fig. 9 Trajectory of torques of hip joint and joints 1 to 3 when the models are equipped with Models A and C. The elastic coefficient is set as $K_p = 200$ Nm/rad, and transition period is T_s is set as 0.15 s

total mass of the model is reduced to utilize the electric servo motor. Figure 10 shows the trajectory of the torque of hip joint when the model equips with rigid body as the trunk when T_s is 0.19 s. Although the model obtains successful transition, peak torque is approximately 1400 Nm, that is twice that of Type A. These results show that the

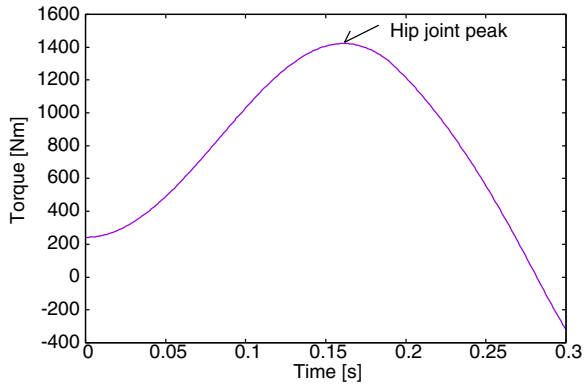

Fig. 10 Trajectory of torque of hip joint when the model equips with the rigid body

proposed trunk mechanism restrains the peak of actuation, and allows the use of a smaller actuator in case of physical operation.

We also observed the feasible range of the period and elastic coefficient of trunk joints with different joint viscosities K_d for Model A. Figure 11a, b show results when the viscosity is set as 1 and 50 Nm/(rad/s), respectively. As shown in the figure, similar distributions are observed. In both cases, a smaller value of the elastic coefficient provides a quicker transition than a rigid body.

Conclusions

This study proposes a novel trunk mechanism with tunable viscoelastic joints for morphological transition from quadrupedalism to bipedalism. The inertia of the trunk significantly influences the transition dynamics. The proposed trunk mechanisms achieve successful quick transition without sensing and precise control but only use a simple PD feedback controller on a hip joint to swing the trunk upward. The comparison of the three trunk models with the rigid body model revealed that a well-designed trunk mechanism with appropriate viscoelastic joints provides quicker transformation than a rigid trunk. In particular, a trunk whose joints are equally distributed or concentrated at the top achieves quicker transition than that of the rigid body. In addition, we determined that the peak torque of the hip joint for swinging up the proposed trunk mechanism is reduced compared to the model equipped with the rigid body. This paper is a first step of the proposed mechanism providing a quick transition, and comprises issues, which will be analyzed in future studies. First, we did not analyze why the trunk mechanism including viscoelastic joints provides quick transition. It is important to discuss the dynamics of the transition. Second, this study dealt with the transition only from quadrupedalism to bipedalism. In the transition, the hip joint generates torques to swing up the trunk against gravity. In contrast, in the transition from bipedalism to quadrupedalism, the gravity contributes to the rapid swing down of the trunk. Third, there are other criteria, such as energy efficiency, compactness, and limitation of the torque for the actuation. Such different phenomena and criteria will be discussed in future. Fourth, this study dealt with a simple model including hip joint only. The influences of the other joints, such as knee, ankle, and shoulder, will be discussed. Lastly, the transition using a physical robot will be investigated in a future study.

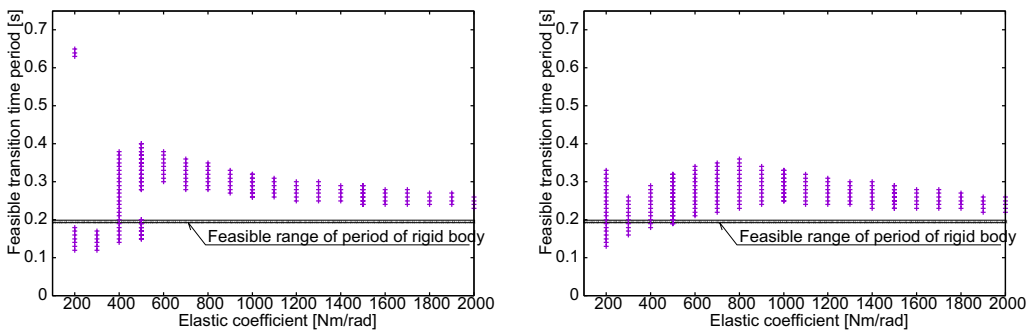

a $K_d = 1.0$ Nm/(rad/s) **b** $K_d = 50.0$ Nm/(rad/s)

Fig. 11 Relationship between elastic coefficient and feasible time period of the transition with different joint viscosities of Model A

Authors' contributions
TT developed the simulation model, carried out the simulation, and drafted the manuscript. WK made a suggestion and comment of the posture transit model. Both authors read and approved the final manuscript.

Acknowledgements
This work was supported by JSPS KAKENHI Grant Number JP16K06201. We'd like to thank to Mr. Keisuke Mitsuda for having fruitful discussion about modeling and simulation.

Received: 20 October 2016 Accepted: 3 March 2017
Published online: 14 March 2017

References

1. Rebula JR, Neuhaus PD, Bonnlander BV, Johnson BJ, Pratt JE (2007) A controller for the littledog quadruped walking on rough terrain, 2007 IEEE international conference on robotics and automation (ICRA), pp 1467–1473
2. Soroewitz A, Kuechler L, Tuleu A, Ajallooeian M, D'Haene M, Moeckel R, Ijspeert AJ (2011) Oncilla robot—a light-weight bio-inspired quadruped robot for fast locomotion in rough terrain, fifth international symposium on adaptive motion of animals and machines, pp 63–64
3. Raibert M, Blankespoor K, Nelson G, Playter R, and the BigDog Team (2008) BigDog, the rough-terrain quadruped robot, 17th world congress the international federation of automatic control (IFAC), pp 10822–10825
4. Gehring C, Bellicoso CD, Coros S, Bloesch M, Fankhauser P, Hutter M, Siegwart R (2015) Dynamic trotting on slopes for quadrupedal robots, 2015 IEEE/RSJ international conference on intelligent robots and systems (IROS), pp 5129–5135
5. Kagami S, Nishiwaki K, Kuffner J, Okada K, Inaba H, Inoue H (2003) Vision-Based 2.5D terrain modeling for humanoid locomotion, proceedings of IEEE international conference on robotics and automation (ICRA), pp 2141–2146
6. Akachi K, Kaneko K, Kanehira N, Ota S, Miyamori G, Hirata M, Kajita S, Kanehiro F (2005) Development of humanoid robot HRP-3P, proceedings of 2005 IEEE/RSJ international conference on humanoid robots, pp 50–55
7. Aoi S, Egi Y, Sugimoto R, Yamashita T, Fujiki S, Tsuchiya K (2012) Functional roles of phase resetting in the gait transition of a biped robot from quadrupedal to bipedal locomotion. IEEE Trans Robot 28(6):1244–1259
8. Asa K, Ishimura K, Wada M (2009) Behavior transition between biped and quadruped walking by using bifurcation. Robot Auton Syst 57(2):155–160
9. Kobayashi T, Aoyama T, Sekiyama K, Fukuda T (2015) Selection algorithm for locomotion based on the evaluation of falling risk. IEEE Trans Robot 31(3):750–765
10. Aoyama T, Kobayashi T, Lu Z, Sekiyama K, Hasegawa Y, Fukuda T (2012) Locomotion transition scheme of multi-locomotion robot, injury and skeletal, biomechanics, pp 21–36
11. Kamioka T, Watabe T, Kanazawa M, Kaneko H, Yoshiike T (2015) Dynamic gait transition between bipedal and quadrupedal locomotion, 2015 IEEE/RSJ international conference on intelligent robots and systems (IROS), pp 2195–2201
12. Wei X, Wang C, Long Y, Wang S (2015) The effect of spine on the bounding dynamic performance of legged system. Adv Robot 29(15):973–987
13. Çulha U, Saranli U (2011) Quadrupedal bounding with an actuated spinal joint, 2011 IEEE international conference on robotics and automation (ICRA), pp 1392–1397
14. Yamasaki R, Ambe Y, Aoi S, Matsuno F (2013) Quadrupedal bounding with spring-damper body joint, 2013 IEEE/RSJ international conference on intelligent robots and systems (IROS), pp 2345–2350
15. Benallegue M, Laumond JP, Berthoz A (2013) Contribution of actuated head and trunk to passive walkers stabilization, IEEE international conference on robotics and automation (ICRA), pp 5638–5648
16. Winter DA (2009) Biomechanics and motor control of human movement, 4th edn
17. Oku H, Asagi N, Takuma T, Masuda T (2015) Passive trunk mechanism for controlling walking behavior of semi-passive walker, 2015 IEEE/RSJ international conference on intelligent robots and systems (IROS), pp 944–949